Nuclear Engineering and Design 141 (1993) 315–328
North-Holland

The use of fluorescence in the measurement of local liquid content in transient multiphase flows

H. Yan *, W.W. Yuen * and T.G. Theofanous

Center for Risk Studies and Safety, Department of Chemical and Nuclear Engineering, University of California, Santa Barbara, CA 93106, USA

Received 1 October 1992

The theoretical basis of a technique we proposed recently for the measurement of local-instantaneous liquid fractions in highly dispersed two-phase flows is developed. The technique is based on the measurement of ultraviolet-induced fluorescence, and the theoretical approach is to carry out numerical experiments accounting for refractions in the radiation transport path and for the randomness in the flow field (i.e., droplet positions and sizes). These numerical experiments indicate that for a properly selected measurement volume (defined by positioning of the fibers) refractions have a small impact and the measurement is predictable and robust. We also present experimental data that demonstrate this excellently predictable behavior.

1. Introduction

The phase content is an essential parameter in two-phase flow, so that a whole field of investigation has been devoted to its measurement [1,2,3]. The work was spawned, especially in the 1970's, by the need to understand in detail a very wide spectrum of transient, non-equilibrium, often multi-dimensional two-phase flows as they occur in a postulated Large Break Loss-of-Coolant Accident in a Light Water Reactor [4]. Early techniques aimed for global measurements (i.e., cross-sectional average), but interest in local measurements began as early as the late sixties and early seventies [5]. At this time, the available instrumentation is wide ranging in principles employed, and highly sophisticated in technique (e.g., double-sensor resistivity probes that measure not only local void fractions but also local interfacial area concentrations) [6,7].

The particular need that led to the investigation and technique reported herein was in measuring the water depletion from the mixing zone prior to a steam explosion. The experiment designed to explore the basic physics of this mixing process involves [8] a cloud of very hot (hundreds of degrees Celsius) particles poured into a liquid (water) volume, and a complex multiphase interaction as the very high steam production drives water out of the mixing region. The situation is highly transient, the flow patterns strongly two-dimensional, and the range of real interest is where the liquid fraction drops below $\sim 20\%$, i.e., the measurement is needed from liquid-continuous to a highly dispersed droplet flow. More generally, the technique is uniquely well suited for multi-dimensional, highly dispersed flows for which both radiation attenuation and the local contact probe techniques fail because of the respective attributes; that is, multi-dimensionality requires a local measurement which is not possible by attenuation methods (even tomography is limited by the conflicting requirement of spatial and temporal resolution), and local contact probes are not suitable for highly dispersed flows. For a good perspective on these matters, see Jones & Delhaye [2].

The basic idea is to induce (in liquid) and detect narrow band emission locally, such that the signal is uniquely related to the quantity of liquid in the detection volume. As described in the original publication [9], we use ultraviolet (UV)-induced fluorescence in combination with fiber optics (see fig. 1) and certain filter/mirror arrangements to achieve:

(1) a good separation between the incident and emitted radiation,

* Also with Department of Mechanical and Environmental Engineering.

(b) a direct relation (not necessarily linear) between liquid fraction and measured signal, and
(c) local, internal measurements in highly complex two-phase flows.

In the previous publication [9], we gave some initial indication of the feasibility of the technique by showing that the power (q) received by the detecting fiber can be expressed as

$$q = I_0 S_f \xi \, e^{-L_1 ac\beta}(1 - e^{-L_e ac\beta})\mathscr{F} \tag{1}$$

and that, for the specific dimensional arrangement as utilized in our experiments, the functional dependence of q on the product $c\beta$ holds well enough that a calibration obtained in 100% liquid ($\beta = 1$), can be applied to highly dispersed droplet flows. That is, the same value of $c\beta$ (with c and β varying independently) gives the same q. In the linear region

$$q = I_0 S_f \xi L_e a \mathscr{F} c\beta \tag{2}$$

and for the same c

$$q/q_{\beta=1} = \beta. \tag{3}$$

The particular instrument has been named FLUTE, for FLUorescence TEchnique.

In this previous publication [9], we also discussed some of the potential difficulties arising from the multiple gas/liquid interfaces within the travel paths of the incident UV and emitted fluorescence beams. Because of the relatively small difference in the index of refraction between water and steam, reflections in this range of wavelength are unimportant [10,11], and this issue came down to the potential role of refractions. In addition, since the high speed data acquisition system allows essentially instantaneous "readings" at rates up to 100 kHz, we discussed the need to optimize the rate in relation to the particular transient under investigation. The purpose of this paper is to pursue further these issues.

Our approach is to conduct numerical experiments of radiation transport, especially accounting for refractions at crossings of interfaces. Random clouds of drops (both positions and sizes) are considered such that with a sufficient number of "realizations", the mean behavior (liquid fraction) can be obtained. More specifically, since the result of each such "realization" corresponds to a FLUTE reading in a physical setting, our effort is to determine (a) whether the average of many such computed "readings" settle to the correct mean value and (b) the number of "readings" required for convergence. Finally, a well-characterized cloud of drops, in an experimental setting, is used to test the predictions of this theory, in a much more precise manner than the feasibility demonstrations provided in the previous paper.

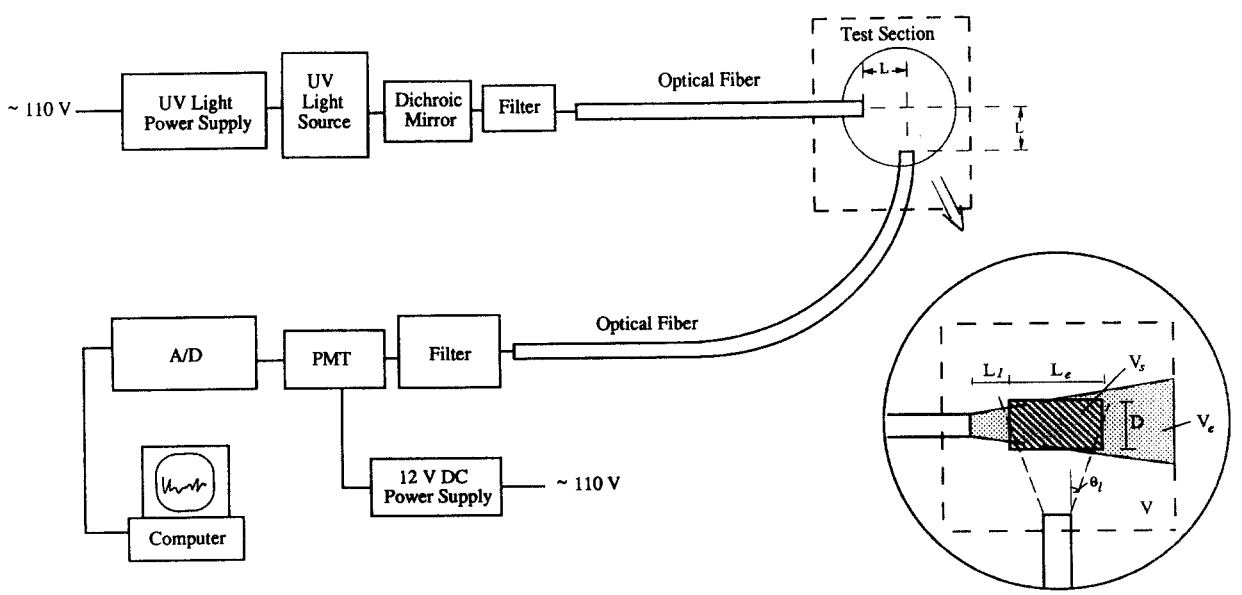

Fig. 1. Illustration of FLUTE arrangement.

2. Theoretical development

2.1. Geometric optics of a FLUTE "reading"

Consider a large cloud of drops. This cloud is characterized by a certain volume-averaged liquid fraction, $\bar{\beta}$, while the local values, β, (defined on any given "sample" volume, V_s) are randomly distributed with a standard deviation σ_β. The spacing between drops is statistically homogeneous and the diameters are normally distributed with a mean $\bar{d}$ and a standard deviation σ_d. Our task is to compute, for a particular cloud arrangement, the radiation received by a fiber tip (defined by its surface area, S_f, and admitting limiting angle, θ_l) due to emissions (fluorescence) from drops found inside a "sample" volume * positioned directly across from the fiber tip at some distance, L, away from it. Since the emissions are isotropic, and of known total intensity, it is sufficient to determine the fraction of the total emitted radiation that is received by the fiber – as noted above, this corresponds to and will be called a FLUTE "reading". Such a "reading" is computed by discretizing the liquid (emitting) volume and the emitted radiation from each volume element, and following a ray-tracing procedure as illustrated in figure 2.

Suppose that E is the total radiative power emitted per unit volume of liquid, and dq_{ei} is the emission

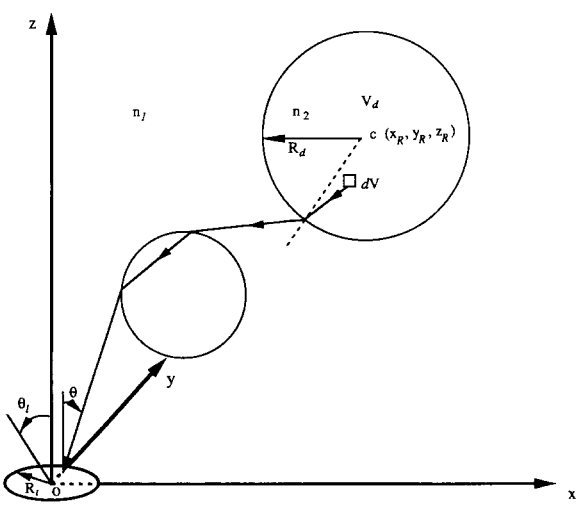

Fig. 2. Illustration of the ray tracing procedure.

* Without loss of generality and very little loss of accuracy, we will assume that all drops emit at the same level of intensity, i.e., will ignore attenuation effects.

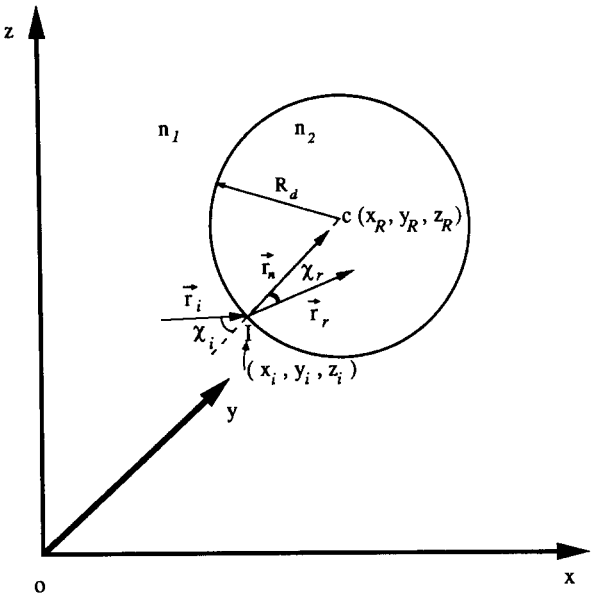

Fig. 3. Nomenclature used in the calculation of a refracted ray.

within the ith solid angle (i.e., 4π discretized to N solid angles, $d\Omega_i$ $i = 1 \ldots N$), then

$$dq_{ei} = E\, dV \frac{d\Omega_i}{4\pi}. \tag{4}$$

Now suppose this radiative power is represented by a single ray (within $d\Omega_i$), take all $d\Omega_i$'s of equal size, and further suppose that N_r of these N rays "hit" (are received by) the fiber. A FLUTE "reading" then is:

$$q = N_r\, dq_{ei} \tag{5}$$

and if $q_{\beta=1}$ is the same quantity calculated for an all-liquid sample volume, the liquid fraction is

$$\beta = q/q_{\beta=1}. \tag{6}$$

Clearly, for accurate results the discretization must be very fine ($N \to \infty$, $dV \to 0$), and this is problematic in computing a large number of "readings", in dense multidrop clouds. The numerical procedure devised to make such computations practical is described in subsection 2.2. In the remainder of this subsection, we describe the ray tracing procedure.

The key element of the ray-tracing calculation is to find the change in direction of a ray crossing the surface of a drop (see fig. 3), which can be treated by geometric optics. Let the unit vectors r_i and r_r represent the incident and refracted direction of the ray

Table 1
Results of sample calculations

Cycle No. [a]	Solid angle $\Delta\Omega$				Size of target (mm)	(q/E) $\times 10^{12}$ (m^3)
	θ_1	θ_2	ϕ_1	ϕ_2		
1 w/o R	0	π	0	2π	1.5	25.83
w R	0	π	0	2π	1.5	14.79
2 w/o R	2.95	π	0	2π	0.5	3.113
w R	2.90	π	0	2π	0.5	3.644
3 w/o R	3.02	π	0	2π	0.5	3.148
w R	3.02	π	0	2π	0.5	3.298

[a] w R and w/o R means "with" and "without" consideration of refractions.

respectively. Relative to a fixed coordinate system, these vectors can be written as

$$\boldsymbol{r}_r = (\sin\theta_i \cos\phi_i, \quad \sin\theta_i \sin\phi_i, \quad \cos\theta_i), \tag{7}$$

$$\boldsymbol{r}_r = (\sin\theta_r \cos\phi_r, \quad \sin\theta_r \sin\phi_r, \quad \cos\theta_r). \tag{8}$$

The unit normal vector at the point of incidence at the surface of the drop, $\boldsymbol{r}_n$, is given by

$$\boldsymbol{r}_n = \left(\frac{x_R - x_i}{R_d}, \frac{y_R - y_i}{R_d}, \frac{z_R - z_i}{R_d}\right). \tag{9}$$

The three vectors, $\boldsymbol{r}_i$, $\boldsymbol{r}_r$ and $\boldsymbol{r}_n$ are related by Snell's law

$$\sin\chi_r = \frac{n_1}{n_2}\sin\chi_i, \tag{10}$$

with

$$\cos\chi_i = \boldsymbol{r}_i \cdot \boldsymbol{r}_n, \tag{11}$$

and

$$\cos\chi_r = \boldsymbol{r}_r \cdot \boldsymbol{r}_n. \tag{12}$$

n_1 and n_2 are the refractive indexes of gas and liquid, respectively. Noting that $\boldsymbol{r}_n$, $\boldsymbol{r}_i$ and $\boldsymbol{r}_r$ are in the same plane, for a given incident direction (θ_i,ϕ_i) and location on the interface (x_i, y_i, z_i), we can readily express the direction of the refracted ray (θ_r and ϕ_r) as follows:

$$\theta_r = \cos^{-1}c' \tag{13}$$

$$\phi_r = \begin{cases} \cos^{-1}\dfrac{a'}{\sqrt{a'^2+b'^2}} & \text{for } b' \geq 0, \\ -\cos^{-1}\dfrac{a'}{\sqrt{a'^2+b'^2}} & \text{for } b' < 0, \end{cases} \tag{14}$$

where

$$a' = A\sin\theta_i\cos\phi_i + B\frac{x_R - x_i}{R_d}, \tag{15}$$

$$b' = A\sin\theta_i\sin\phi_i + B\frac{y_R - y_i}{R_d}, \tag{16}$$

$$c' = A\cos\theta_i + B\frac{z_R - z_i}{R_d}, \tag{17}$$

with

$$A = \frac{\sin\chi_r}{\sin\chi_i}, \tag{18}$$

and

$$B = \frac{\sin(\chi_i - \chi_r)}{\sin\chi_i}. \tag{19}$$

2.2. Computational procedure

As noted above, for accurate results we must consider a high enough density of emitted energy rays, and this gives rise to serious constraints of implementation, even for main frame computers. To overcome this difficulty, we developed an adaptive numerical approach that is made to successively focus (or "cluster") the emissions to the region of interest; that is, to the emission solid angle space (say $\Delta\Omega$) that produces "hits". This successive focusing proved possible and allowed us to achieve high enough ray densities with reasonable computational effort.

Specifically, the computation starts by first emitting N rays (for each differential volume dV) randomly (but uniformly) over the full solid angle 4π. By mapping the direction of the intercepted (received) energy rays on a (θ, ϕ) plane, the clustering is evident and the first estimate of the region of interest, say $\theta_1 < \theta < \theta_2$, $\phi_1 < \phi < \phi_2$, can be readily generated. A second calculation is then performed by emitting N rays randomly and uniformly only within the region of interest determined in the previous step. The procedure is then repeated until convergence is achieved. To ensure that the first deduction in θ_1, θ_2, ϕ_1 and ϕ_2 is conservative, the hits are computed with a target diameter three times bigger than the one of interest. For $N = 1000$ we have found that only 3 such cycles of computation can produce an adequate focus (on the region of interest). Moreover, we have shown that the choice of 1000 rays over the region of interest produces a fine enough discretization for convergence in the "reading" itself.

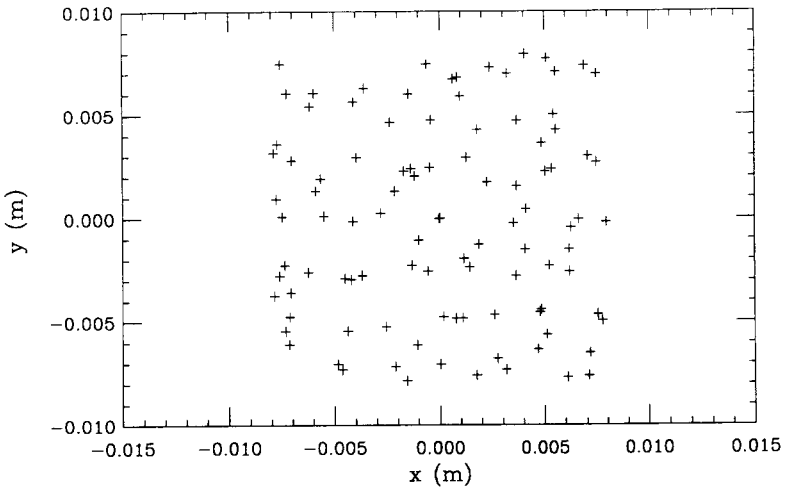

Fig. 4. Drop positions projected on the $x-y$ plane.

Specific illustrations of this technique are provided in the next section.

3. Numerical experiments

To illustrate the numerical procedure as outlined in the previous section, energy emitted by a single drop in a cloud of 100 uniformly-sized drops is first considered. The cloud of 100 drops was formed by randomly positioning the centers in the cube $-8 < x < 8$, $-8 < y < 8$ and $0 < z < 16$; all dimensions in mm. The drops have a diameter of 2.64 mm and the average liquid fraction is 15%. The emitting drop, same size, is positioned at (0, 0, 13.7). The calculations are carried out by discretizing the emitting drop into 64 small volumes and considering 1000 rays emitted from each volume, in each cycle. The results of three successive cycles are summarized in table 1. Results generated ignoring the effect of refraction are shown in the same table. Note that for the case without refraction, the exact value of q/E can be determined analytically and it is $3.15\times$

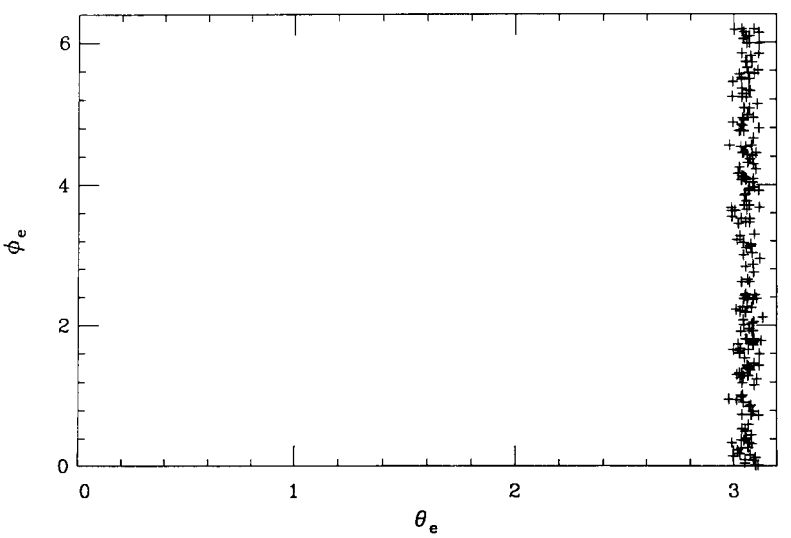

Fig. 5. Clustering in $\theta-\phi$ space for cycle No. 1 w/o R.

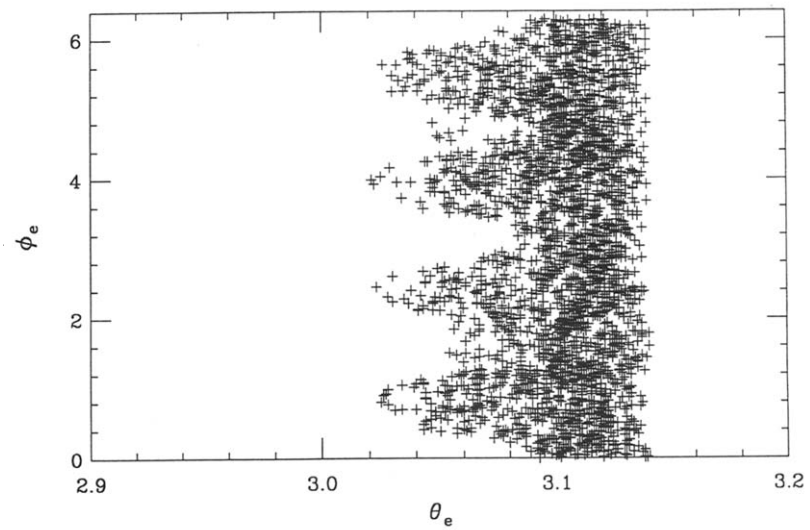

Fig. 6. Clustering in $\theta-\phi$ space for cycle No. 2 w/o R.

10^{-12} m^3. The computational procedure is clearly both accurate and efficient. To generate the same accuracy as cycle 3, for example, a "straight" calculation with uniform emission over 4π would require 10^6 rays per volume element, dV – as opposed to 3,000 rays used to arrive at the table 1 result. The drop positions projected on the x–y plane are shown in fig. 4. Figures 5 to 10 correspond to each computational run of table 1 and show the clustering (in θ–ϕ space) of the emitted rays that hit the target. They also show the process of "focussing-down" of $\Delta\Omega$ to the proper region of interest – this focussing is done automatically by the computer. With reference to these figures, and table 1, the following points can be made.

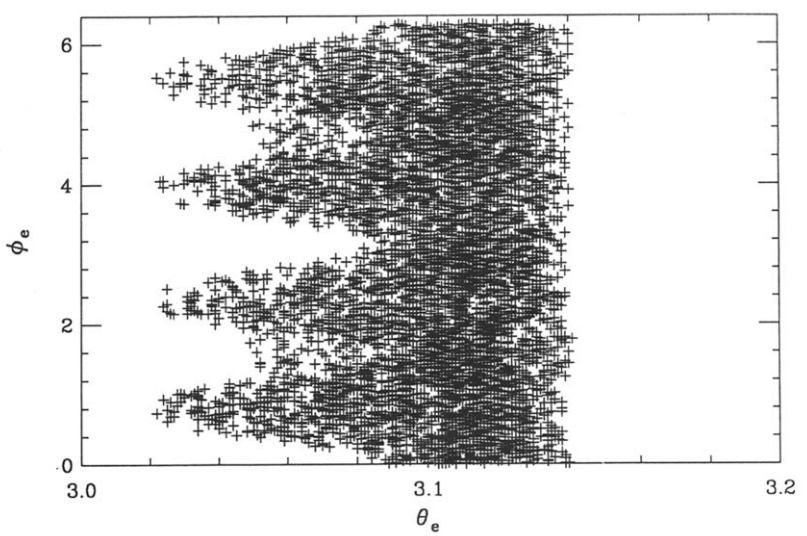

Fig. 7. Clustering in $\theta-\phi$ space for cycle No. 3 w/o R.

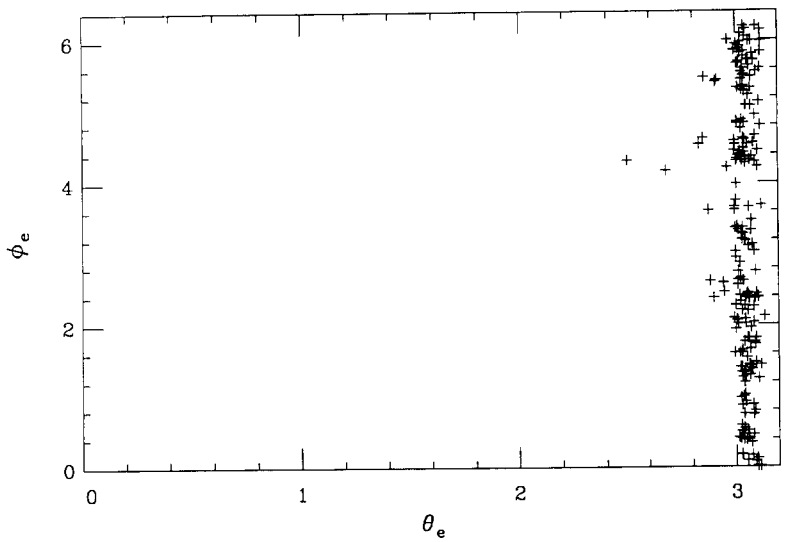

Fig. 8. Clustering in $\theta-\phi$ space for cycle No. 1 w R.

(1) The clustering is rather sharp and allows an unambiguous choice of the area to focus on the next cycle.
(2) No significant clustering is observed in the ϕ dimension, because of the symmetric position of the drop right in front of the target; off-the-side positions would create ϕ-clustering also.
(3) The regular "hit" pattern in figs. 6 and 7 is probably due to the symmetry of discretizing the emitting drop ($4 \times 4 \times 4$) which in the absence of refractions shows through. Additional studies are required to understand the physical significance of this pattern. As seen in figs. 9 and 10 refractions "randomize" the behavior sufficiently to destroy this pattern.
(4) For this particular realization the effect of refractions is to increase the "reading" by less than 5%.

Turning next to the general problem, the key parameters to consider are:

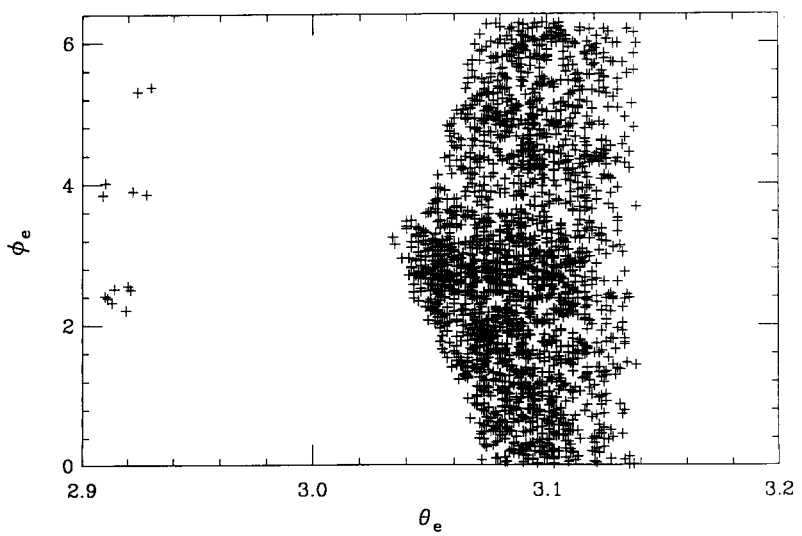

Fig. 9. Clustering in $\theta-\phi$ space for cycle No. 2 w R.

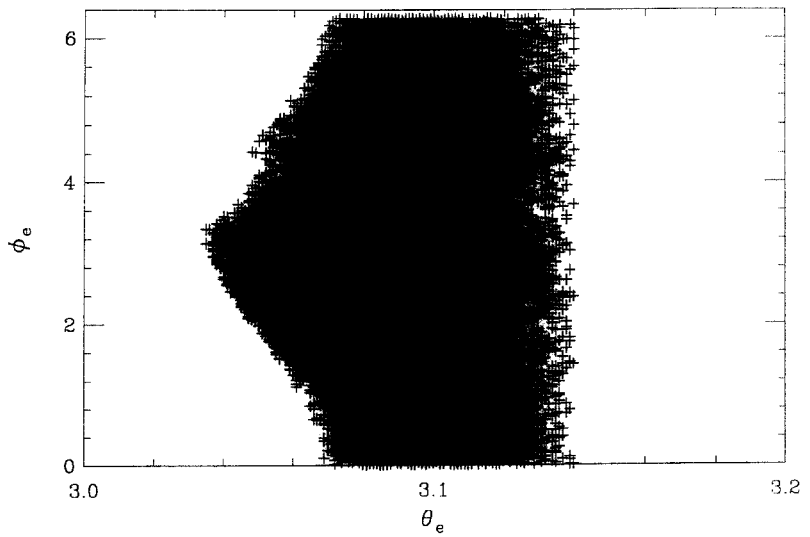

Fig. 10. Clustering in $\theta-\phi$ space for cycle No. 3 w R.

$\bar{\beta}$ the liquid fraction in a cloud of volume V,
σ_β the standard deviation of liquid fraction for a sample volume V_s,
$\bar{d}$, σ_d mean and standard deviation of droplet size distribution,
S_f, θ_l area and maximum admitting angle of fiber tip,
V_s, L sample volume and distance of its center from target.

Using numerical experiments of the type illustrated above, our purpose here is to predict and optimize the performance of FLUTE in terms of appropriate ranges of these parameters. In particular, we wish to establish any limitations due to the refractions (the issue raised in the introduction) and/or due to the particular geometry of the "emitting" volume, V_e. This latter point requires some further elaboration. The relation of the "emitting" and "sample" volumes in FLUTE is illustrated in fig. 1 – the issue is whether there is an apparent increase of sample volume, due to refractions, from emissions outside it, or whether in some

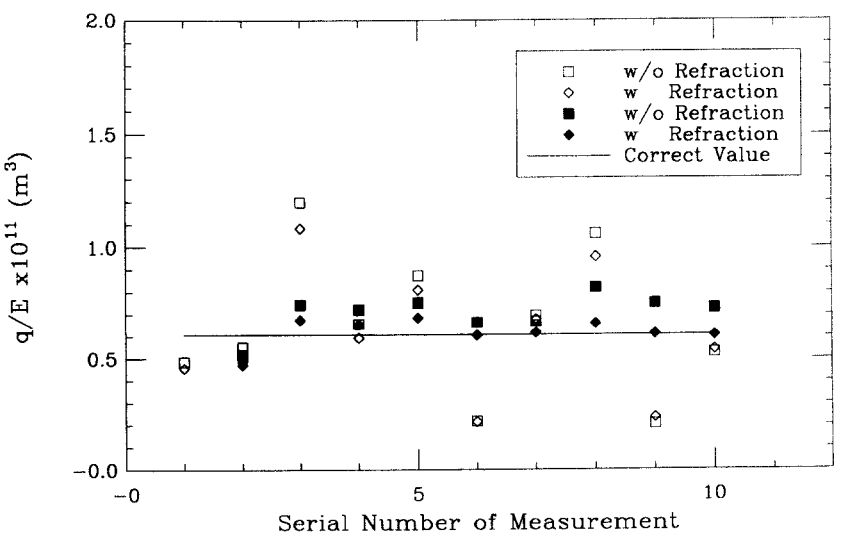

Fig. 11. Results of Run #1. ■ and ◆ are the averages of all previous readings.

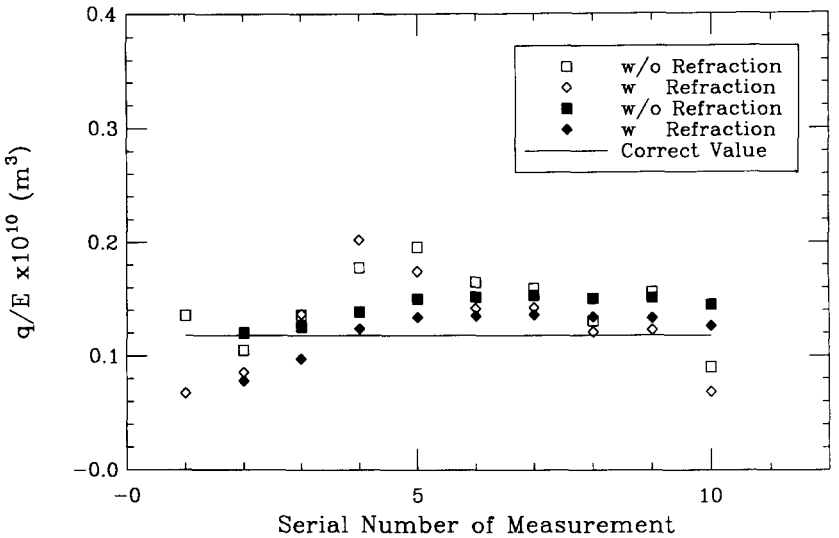

Fig. 12. Results of Run #2. ■ and ◆ are the averages of all previous readings.

average sense such a gain is cancelled by an equivalent loss (again by refractions) of the emitted radiation within. A particular choice of V_s and L implies an equivalent diameter, D, of a pencil of UV radiation. This then is the diameter of the emitting volume and the emitting volume can be parametrized by one more variable, the effective length of it, L_e. We will show shortly that any increases of L_e beyond the value determined from the geometric intersection of receiving fiber with the UV pencil, produce a negligible effect. Thus we chose and fixed $L = 10$ mm, $L_e = 8$ mm, $\theta_l = 22°$, and $R_f = 0.5$ mm, thus focusing this study on $\bar{\beta}$, $\bar{d}$, and σ_d. The matrix of variations considered is shown in table 2. Each run involved 10 successive "readings", each "reading" or computation carried for a new, randomly arranged cloud, with the

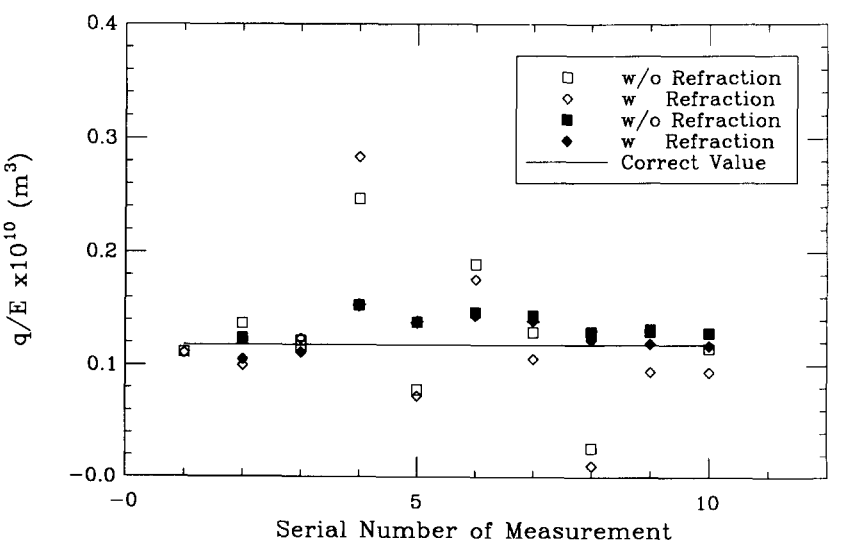

Fig. 13. Results of Run #3. ■ and ◆ are the averages of all previous readings.

Table 2
The matrix of parameters in the calculations (in all runs $L = 10$ mm, $L_e = 8$ mm, $\theta_l = 22°$)

Run #	$\bar{\beta}$(%)	$\bar{d}$(mm)	σ_d(mm)
1	3.0	1.2	0.3
2	5.5	1.2	0.3
3	5.5	2.4	0.3
4	14.0	2.4	0.3

parameters as specified. For each cloud two computations were run – one with and the other without considering refractions.

The results are summarized in figs. 11 to 14. The figures show the successive readings and the "current" average (i.e. the average of all previous readings). The correct values, based on the known liquid fraction, and taken as the same fraction of the "reading" at 100%

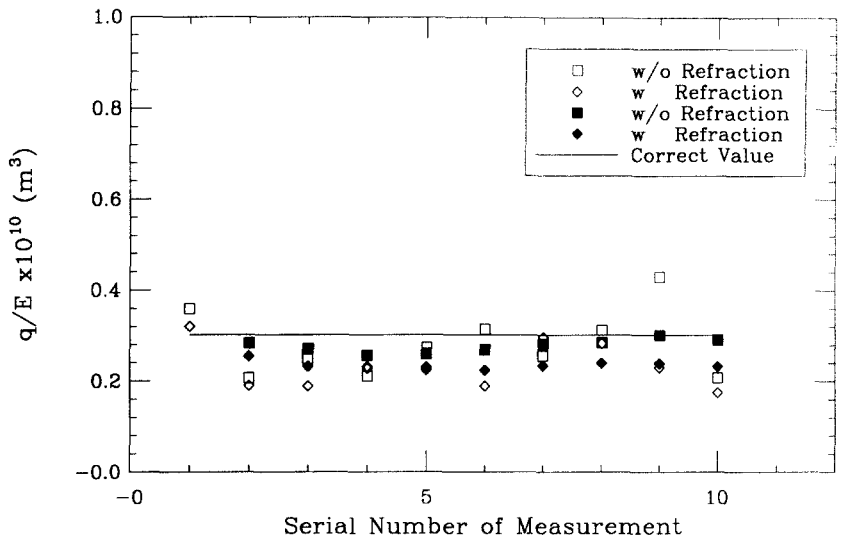

Fig. 14. Results of Run #4. ■ and ◆ are the averages of all previous readings.

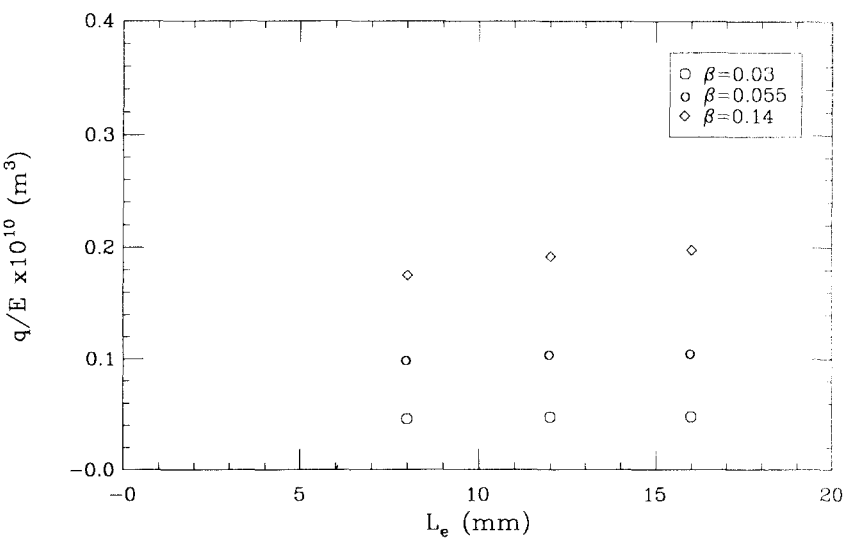

Fig. 15. Effect of L_e on "readings" with refraction consideration.

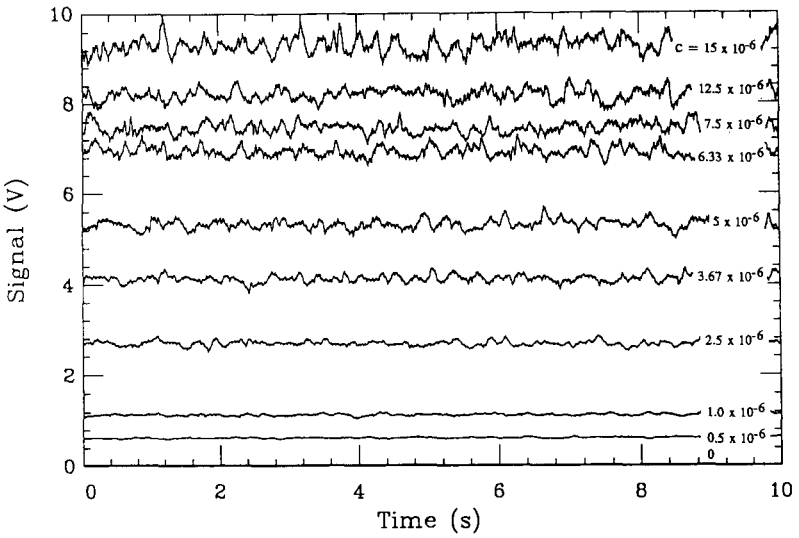

Fig. 16. Experimental signals for varying dye mass fraction in 100% water.

liquid, are also shown. There are two main observations: (a) the fluctuations are significant, but the average reading quickly converges to the correct value, and (b) the effect of refractions for $\beta < 0.1$ is negligible. To illustrate the effective length L_e, the first "reading" of Run #1, the second "reading" of Run #3 and the last "reading" of Run #4 were repeated with L_e taken as 12 and 16 mm and results are shown in fig. 15. We see that the effect of increasing L_e (symmetrically around the geometrically determined minimum value) has no significant consequence on the results.

4. Laboratory experiments

The approach here is similar to that employed in the original publication [9]. That is, to create a well-controlled, uniform cloud of particles of known liquid

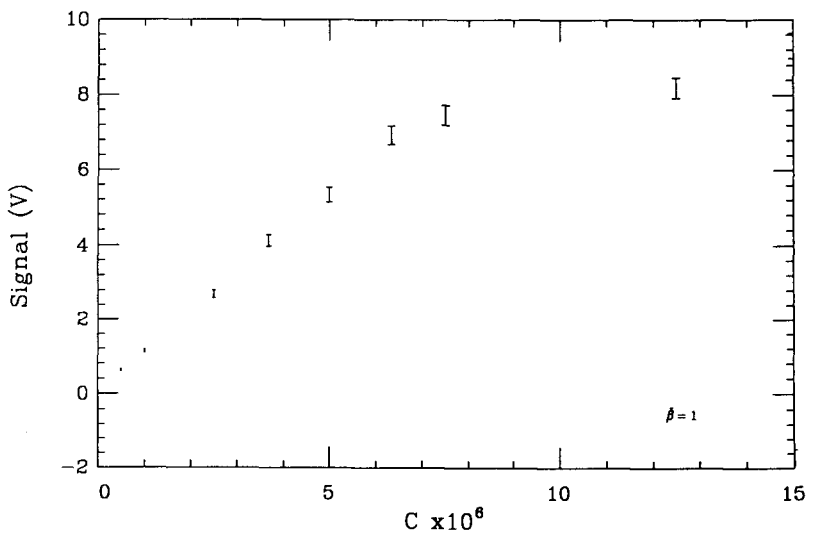

Fig. 17. FLUTE signal in 100% water as function of the dye mass fraction content.

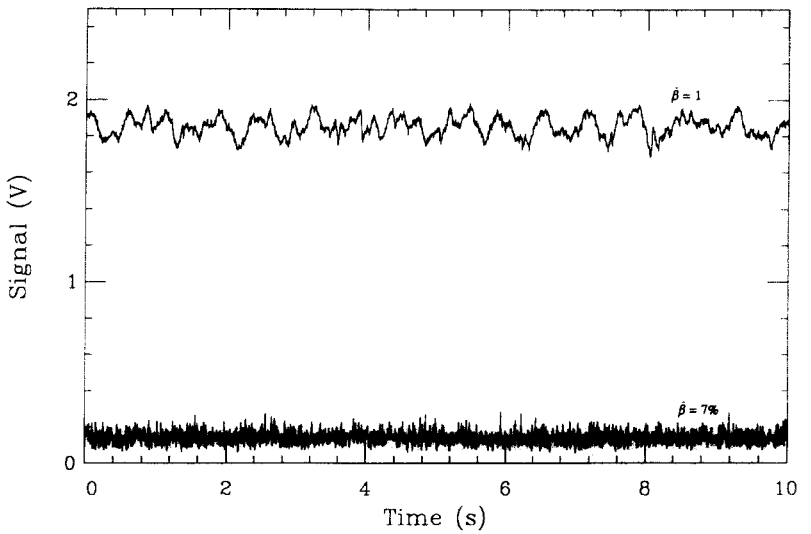

Fig. 18. FLUTE signals obtained in droplet flow (with $\bar{\beta} = 0.07$) and in all liquid ($\bar{\beta} = 1.0$).

fractions, and to test the $q - c\beta$ relation of eq. (1). The cloud is created by letting water flow through a perforated disc under a constant driving head. In the previous study we found some non-uniformity (in the flow) developing with distance along the free-fall due to small imperfections, in hole pattern, etc. For the present work, we chose the best disc, visually, and from close-up photographs we determined the position where the jets first disintegrated into drops. This is an ideal position for a local measurement with a known liquid fraction. The fiber positioning was set at $L = 10$ mm and the FLUTE sampling rate at 200 Hz.

The experimental signal from a series of calibration runs (varying the concentration of the dye), and the resulting calibration curve are shown in figs. 16 and 17, respectively. Figure 17 clearly shows the linear region of eq. (1). The signals obtained in the droplet flow described above at liquid fractions of 7% and 8.5% are

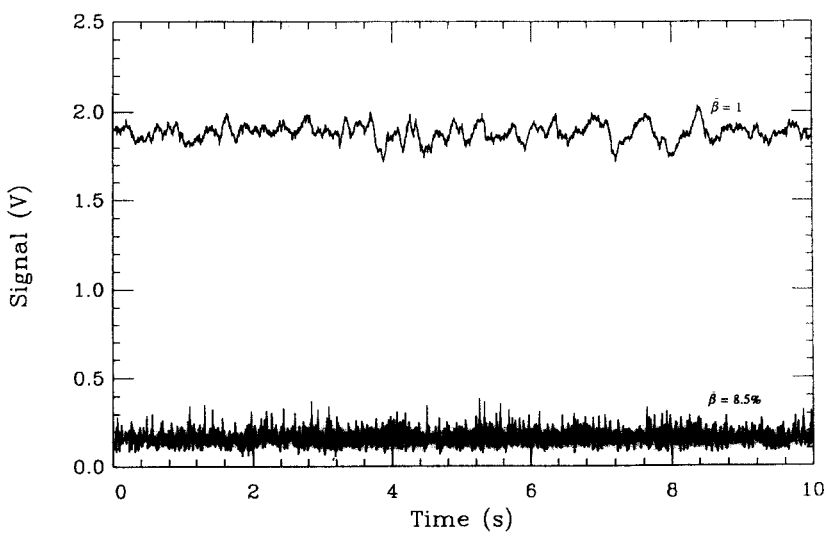

Fig. 19. FLUTE signals obtained in droplet flow (with $\bar{\beta} = 0.085$) and in all liquid ($\bar{\beta} = 1.0$).

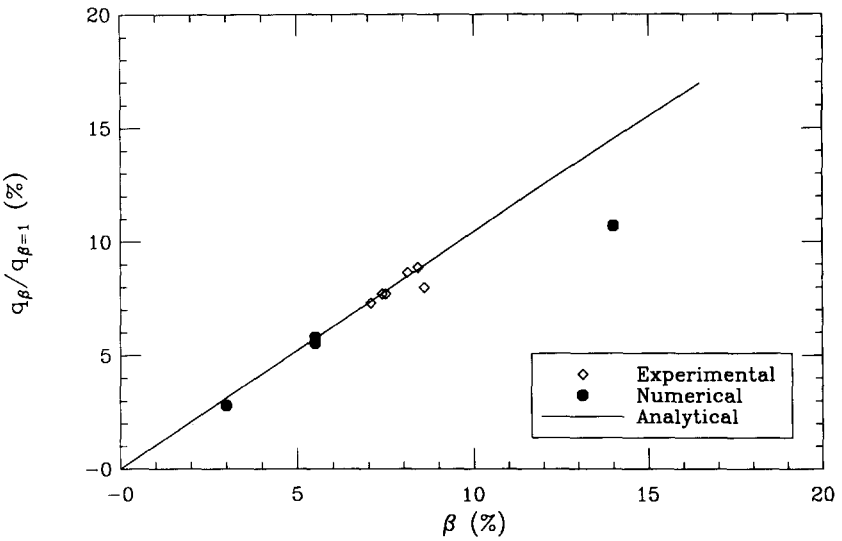

Fig. 20. Comparison between experimental results and numerical simulations. The solid line (analytical) reflects linearity as in eq. (3).

shown in figs. 18 and 19, respectively. The average values obtained from these signals (and several others obtained in the same range of liquid fractions), normalized by the signals in 100% liquid (also shown in figs. 18 and 19), are shown in fig. 20, plotted against the respective (known) liquid fractions. The "numerical" data on this figure are those obtained in the numerical simulations discussed above. The solid line expresses an ideally linear relation, i.e., $q \sim \beta$, as deduced from the linear region of eq. (1). We see that at the high end of the liquid fraction considered refractions are predicted to introduce non-negligible errors; however, the performance is excellent at the low end, and it is predicted to be in excellent agreement with the measurements. [Note that the non-linearity exhibited by the numerical experiments is not the same as that of eq. (1) – the latter is due to attenuation.] Further experimental work and numerical simulations are needed to fully explore the range of validity of FLUTE at liquid fractions higher than 10%; however, it should also be noted that the dispersivity in this range is expected to diminish (by drop coalescence) providing an inherent limitation on the errors due to refractions.

5. Conclusions

In this paper we provide the theoretical foundation of FLUTE, and basically an explanation of why it "works". In particular, we have shown that for $\beta < 0.1$ the role of refractions on the reliability of the signal is negligible, and that random clouds of drops (of distributed size) can be characterized by the average of only a few measurements. This means the technique is applicable also to highly transient flows, with varying liquid content.

Acknowledgments

This work was performed for the U.S. Nuclear Regulatory Commission under contract No. 0489-082.

Nomenclature

a	absorption coefficient of ultra-violet radiation,
c	mass fraction of dye in water,
$\bar{d}$	mean drop diameter,
D	diameter of emitting volume,
E	radiant power emitted per unit volume,
$\mathscr{F}$	geometric optic factor,
I_0	exciting-light intensity,
L	distance of center of sample volume from target,
L_e	effective length of emitting volume,
n_i	index of refraction of medium i,
N	number of emitted rays,
N_r	number of rays received by target,
q	total radiant power received by target,

r, θ, ϕ spherical coordinates,
$\boldsymbol{r}$ unit vector,
R_d drop radius,
R_t radius of target (fiber),
S_f surface area of target (fiber),
V volume of droplet cloud,
V_d volume of a droplet,
V_s sample volume of emitting drops in a cloud,
x, y, z cartesian coordinates.

Greek

$\bar{\beta}$ liquid fraction in a droplet cloud,
θ_l maximum admitting angle by target (fiber),
σ_β standard deviation of liquid fraction in V_s,
σ_d standard deviation of drop diameter distribution,
ξ quantum of yield of dye,
χ angle between normal and incident or refracted directions.

Subscripts

e emitting volume,
i incident,
n normal,
r refracted,
R position of a drop center.

References

[1] G.F. Hewitt, Measurement of Two Phasse Flow Parameters (Academic Press, London, 1978).
[2] O.W. Jones and J.M. Delhaye, Transient and statistical measurement techniques for two-phase flows: a critical review, Int. J. Multiphase Flow 3 (1976) 89–116.
[3] J.M. Delhaye and G. Cognet, eds., Measuring Tecniques in Gas-Liquid Two-Phase Flows (Springer-Verlag, 1984).
[4] A.L. Hon, D. Basdekas, Y.Y. Hsu, N. Kondic and R. van Houten, eds., Review Group Conference on Advanced Instrumentation Research for Reactor Safety, NUREG/CP-0015 (1980).
[5] J.M. Delhaye, R. Semeria and J.C. Flamand, Void fraction and vapor and liquid temperatures: local measurements in two-phase flow using a microthermocouple, J. Heat Trans. (1973) 365–370.
[6] Z. Wang and G. Kocamustafaogullari, Interfacial characteristic measurements in a horizontal bubbly two-phase flow, ANS Proceedings, Winter Meeting, Washington, D.C., 1990.
[7] M. Ishii and S.T. Revankar, Measurement of local interfacial area and velocity in bubbly flow, ANS Proceedings 1991 National Heat Transfer Conference, Vol. 5 (1991) 181–189.
[8] W.H. Amarasooriya and T.G. Theofanous, Scaling considerations in steam explosions, ANS Proceedings 1987 National Heat Transfer Conference, Vol. 2 (1987) 58–67.
[9] S. Angelini, W.M. Quam, W.W. Yuen and T.G. Theofanous, FLUTE: FLUorescence TEchnique for two-phase-flow liquid-fraction measurements, Proc. ANS 1991 Winter Meeting, San Francisco, 1991, Chemical Engineering Communications 118 (1992) 237–249.
[10] G.M. Hale and M.R. Querry, Optical constants of water in the 200-m to 200 μm wavelength region, Applied Optics 12, No. 3 (March 1973) 555.
[11] R. Siegel and J.R. Howell, Thermal Radiation Heat Transfer, second edition (Hemisphere Publishing Co., London, 1981).